reported here were measured at 300 and 10 K to be consistent with the IINS data. Polarization studies were also made with a saturated $CHCl_3$ solution.

Inelastic Neutron Scattering Spectra. IINS measurements at BNL were carried out at the High Flux Beam Reactor, using a triple-axis spectrometer. Low-energy spectra were obtained with pyrolytic graphite (002) for both monochromator and analyzer crystals and a BF_3 proportional counter detector. Data were measured at a fixed **q** for constant monitor counts. High-energy spectra were obtained with a beryllium (002 and 110) monochromator and a liquid-nitrogen-cooled beryllium filter analyzer (cutoff energy of 5.2 meV and mean band-pass of ~3.5 meV). Substantial gains in counting rates should be possible with a beryllium filter analyzer with a larger solid angle of acceptance. The polycrystalline sample of $Mn(CO)_5CH_3$ (10.6 g) was mounted in a cylindrical aluminum can 1.9 cm in diameter maintained at 9 K. Transmission measurements showed that the sample scattered 75% of the incident neutrons.

A revised sample holder was prepared prior to data collection at Los Alamos to decrease the degree of multiple scattering. A 27.6-g sample of $Mn(CO)_5CH_3$ was mounted in an annular geometry in a cylindrical aluminum can (0.93 in. i.d.) whose center was kept hollow by a second aluminum cylinder (0.625 in. o.d.). The IINS measurements at Los Alamos were then carried out at ~10 K by using the WNR pulsed-spallation neutron source and a beryllium filter analyzer time-of-flight spectrometer. The instrument used in the present experiment is a prototype[34] of a more elaborate version currently under development at the WNR. The incident and final flight paths were 11.42 and 0.26 m, repectively, which, along with the filter band-pass, primarily determine the energy resolution of approximately 12% ($\Delta E/E$) at 150 meV. Three adjacent pie-shaped Be filter sections, each 15 cm long, were centered at 72°, 90°, and 108° scattering angles from the sample. Each of these filter sections was viewed by six ^3He counters and time analyzed separately from each other in order to correct for variations in backgrounds. Frame overlap was eliminated with a gadolinium foil filter. After background subtraction and correction for filter transmission factors, the spectra were divided by the spectrum of incident neutrons and related to the scattering function $S(Q, \omega)$ which is the quantity plotted in the figures.

(34) Eckert, J.; Silver, R. N.; Soper, A. K.; Vergamini, P. S.; Goldstone, J. A.; Larson, A. C.; Seeger, P. A.; Yarnell, J. *Proc. Int. Collab. Adv. Neutron Sources, 4th* **1981** (KENS Report II).

Acknowledgment. We are grateful for the assistance of Dr. Graheme Williams in the X-ray diffraction study of $Mn(CO)_5CH_3$ and to Professors T. Spiro and H. Kaesz for helpful discussions. The work reported here was carried out at the Brookhaven and Los Alamos National Laboratories under contract with the U.S. Department of Energy.

Registry No. $Mn(CO)_5CH_3$, 13601-24-6; $Mn(CO)_5CD_3$, 15653-52-8.

Supplementary Material Available: IR and Raman spectra of $Mn(CO)_5CD_3$ (Figures 1S–4S), IINS spectra of $Mn(CO)_5CH_3$ (Figures 6S–9S), pictoral representations of internal vibrational symmetry coordinates (Figure 5S), and vibrational overtone and combination frequencies for $Mn(CO)_5CH_3$ (Tables IS–IIIS) (20 pages). Ordering information is given on any current masthead page.

X-ray Absorption Spectra of Ruthenium L Edges in $Ru(NH_3)_6Cl_3$

T. K. Sham

Contribution from the Department of Chemistry, Brookhaven National Laboratory, Upton, New York 11973. *Received June 21, 1982*

Abstract: X-ray absorption spectra of ruthenium L edges of $[Ru(NH_3)_6]Cl_3$ have been obtained with synchrotron radiation. It is found that Ru L edges exhibit white lines characteristic of ligand-field and spin–orbit effects. Analysis of the data on the basis of local symmetry and the electronic configuration of the complex yields a $10Dq$ value of 3.93 eV.

Recent advances in synchrotron radiation technology have opened up new avenues for studying X-ray excitation of core electrons into the empty valence levels (discrete bound states) and the continuum.[1-10] In a typical X-ray absorption experiment, the absorption coefficient of a particular edge as a function of the photon energy below and above the ionization threshold is measured. In condensed matter studies transitions from the core level to the valence levels often produce structures at the edge characteristic of the local symmetry and electronic configuration of the atom; transitions to the continuum, on the other hand, give rise to oscillations in the absorption coefficient up to as much as 1000 eV above the threshold. The latter phenomenon is called extended X-ray absorption fine structure (EXAFS) and has been well understood,[1-10] while studies of the near-edge region with synchrotron radiation remain relatively limited.[4,11-14] Recently,

(1) Eisenberger, P.; Kincaid, B. M. *Science (Washington, D.C.)* **1978**, *200*, 1441 and reference therein.
(2) Stern, E. A. *Contemp. Phys.* **1978**, *19*, 289.
(3) Winick, H.; Bienenstock, A. *Annu. Rev. Nucl. Part. Sci.* **1979**, *28*, 33. Watson, R. E.; Perlman, M. L. *Science (Washington, D.C.)* **1978**, *199*, 1295. Kunz, C., Ed. "Synchrotron radiation-techniques and applications" Springer-Verlag: New York, 1979.
(4) Shulman, R. G.; Yafet, Y.; Eisenberger, P.; Blumberg, W. E. *Proc. Natl. Acad. Sci. U.S.A.* **1976**, *73* 1384.
(5) Cramer, S. P.; Hodgsen, K. O.; Stiefel, E. I.; Newton, W. E. *J. Am. Chem. Soc.* **1978**, *100*, 2748. Cramer, S. P. Ph.D. Thesis, Stanford University, 1978.
(6) Brown, M.; Peierls, R. E.; Stern, E. A. *Phys. Rev. B: Solid State* **1977**, *15*, 738.
(7) Citrin, P. H.; Eisenberger, P.; Kincaid, B. M. *Phys. Rev. Lett.* **1976**, *36*, 1346.
(8) Teo, B. K.; Lee, P. A. *J. Am. Chem. Soc.* **1979**, *101*, 2915.
(9) Stern, E. A.; Sayers, D. E.; Lytle, F. W. *Phys. Rev. Lett.* **1976**, *35*, 298.
(10) Brown, F. C.; Backrach, R. Z.; Bianconi, A. *Chem. Phys. Lett.* **1978**, *54*, 425.
(11) Early edge studies carried out before the synchrotron radiation era was documented: Srivastava, U. C. and Nigam, H. L. *Coord. Chem. Rev.* **1972–1973**, *9*, 275. For the advantage of synchrotron radiation over conventional source, see ref 1–3.
(12) Brown (Brown, F. C. *Solid State Phys.* **1974**, *29*, 1) reviewed early synchrotron work of outer edges.

0002-7863/83/1505-2269$01.50/0

Table I. Electric Dipole Allowed Transitions in $Ru(NH_3)_6Cl_3$ L-Edge Absorption[a]

edge	atomic notation	initial state symmetry	dipole operator r	final state (allowed) symmetry			
				5s	5p	$4d_{xy,yz,xz}$	$4d_{x^2-y^2,z^2}$
L_I	2s	a_1	t_1		t_1		
$L_{II,III}$	$2p_{1/2,3/2}$	t_1	t_1	a_1		t_2 (ζ,ξ,η)	e (v,u)

[a] Only local symmetry O is considered; ν, u, ζ, ξ, and η are the octahedral basis functions in terms of spherical harmonics ($u = Y_{20}$, $\nu = (1/2)^{1/2}(Y_{22} + Y_{2-2})$, $\xi = i(1/2)^{1/2}(Y_{21} + Y_{2-1})$, $\eta = (1/2)^{1/2}(-Y_{21} + Y_{2-1})$, and $\zeta = i(1/2)^{1/2}(-Y_{22} + Y_{2-2})$).

ruthenium complexes have become subjects of considerable interest in connection with the structural and electronic aspects of kinetics and mechanisms of electron-exchange reactions.[15] The L-edge spectra of Ru in $[Ru(NH_3)_6]Cl_3$ have been recorded at Stanford Synchrotron Radiation Laboratory (SSRL). The results of this study are reported here in some detail.

In the edge region a very sharp peak (or peaks) is sometimes observed. This feature is often called the "white line" for historical reasons.[16] These peaks arise primarily from atomic-like electric dipole transitions (change of angular momentum $\Delta l = \pm 1$). In L-edge absorption, one would expect transitions from 2s (L_I) to unoccupied p states and from $p_{1/2}$ (L_{II}) and $p_{3/2}$ (L_{III}) to unoccupied states of both s ($\Delta l = -1$) and d ($\Delta l = 1$) symmetry.[6,9] The intensity and shape of these transitions depend upon the transition probability, i.e., the dipole transition matrix elements involving the initial and final state wave functions (ψ_i and ψ_f), and the distribution of the density of states.

Strictly speaking, the unoccupied final states in X-ray absorption do not have the atomic symmetry in the condensed phase. However, the initial states, such as the K and L_I core levels, are essentially atomic. White lines at the K and L_I near edge, for example, must be caused by transitions to the unoccupied valence states containing mostly p character of the absorbing atom and having the proper symmetry defined by the molecular environment (energy bands in metals and molecular orbitals in molecules). Since the outermost atomic orbitals are modified considerably in the condense phase, white lines of different nature may arise depending upon the nature of the bonding. In semiconductors, the core hole produced by X-ray absorption is unscreened and a stable electron-core hole pair is formed. Transition to such excitation levels[6,17] would produce intense and narrow absorption peaks at the edge.[6,12,17] In simple metals, such as Al and Mg, manybody effects[13] are responsible for $L_{II,III}$-edge white lines. In transition metals and their complexes, such as the one described here, the white lines are attributed to transitions to localized, unoccupied states.

Experimental Section

All the Ru L-edge spectra were recorded in a transmission mode with the focused EXAFS spectrometer at SSRL with SPEAR running at 3.2 GeV. Si(111) crystals were used in a double-crystal monochromator. This spectrometer has an effective photon energy range of 2800–~9500 eV (due to focussing mirror cutoff at ~9.5 keV). The resolution is ~5 eV at the high energy limit and ~2 eV at the lower energy limit for our measurements. Spectra were recorded at room temperature with the sample cell sandwiched between the first (I_0) and second (I) ionization chamber, to minimize air absorption. Helium was used in I_0 and N_2 in I. Higher harmonics were supressed by detuning the spectrometer to 30% of its maximum intensity at ~3 keV. Several spectra were taken for each edge to ensure reproducibility. The specimen was prepared in the form of a homogeneous mixture of finely ground powder of $[Ru(NH_3)_6]Cl_3$ and grease Vaseline. The mixture was then flattened between two Kapton windows (0.125×10^{-3} in.). Individual I_0 and I measurements were made during each scan.

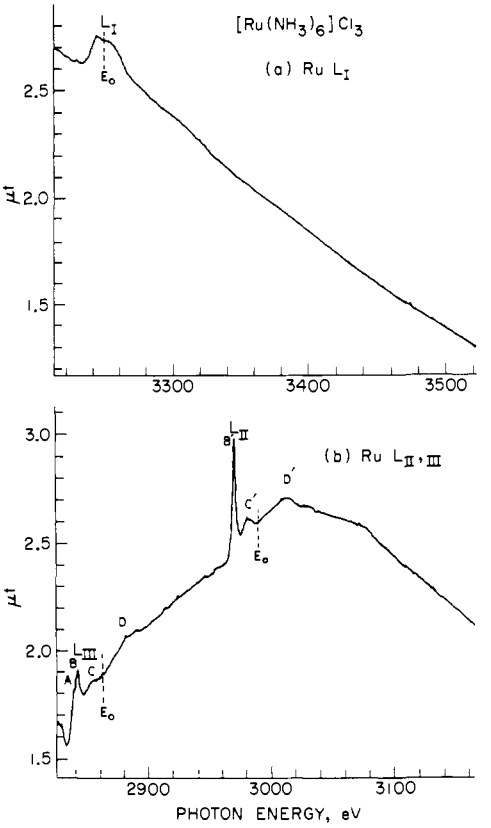

Figure 1. X-ray absorption spectra of the ruthenium L_I (a) and $L_{II,III}$ edges (b); E_0's are obtained by a procedure described in the text.

Results

The L_I spectrum (Figure 1a) shows two very weak peaks just before the edge jump followed by an intense transition and a broad structure. At higher energies, several oscillations characteristic of the EXAFS are observed. The $L_{II,III}$ spectrum (Figure 1b) exhibits relatively narrow and intense absorption peaks in the near-edge region in contrast to the broad L_I edge. The small double-peak structure at ~2820 eV is the Cl K edge of which the EXAFS contributes somewhat to the rising background of the L_{III} edge. Detail near-edge features are shown in Figure 2.

Ionization threshold E_0 of the Ru L_I edge was obtained from EXAFS analysis (vide infra). The E_0's of $L_{II,III}$ were obtained by aligning the theoretical edge positions tabulated by McMaster et al.,[18] with E_0 determined for the L_I edge by EXAFS analysis (Figure 5; vide infra). The positions of these E_0's immediately suggest that the resonance peaks below E_0 must arise from bound state to bound state transition.

Qualitative Assignment. These edge features can be discussed on the basis of the local molecular symmetry of the complex and the dipole transition approximation. Let us consider for the moment the local symmetry of an octahedral complex of Ru^{3+} with six identical σ-type ligands. The valence states of the metal ion transform as A_1 (s), T_1 ($p_{x,y,z}$), E (d_{z^2}, $d_{x^2-y^2}$), and T_2 (d_{xy}, d_{yz},

(13) Mahan, G. D. *Solid State Phys.* **1974**, *29*, 75.
(14) Dehmer, J. L.; Dill, D. *J. Chem. Phys.* **1977**, *65*, 5327. Kutzler, F. W.; Natoli, C. R.; Misemer, D. K.; Doniach, S.; Hodgson, K. O. *Ibid.* **1980**, *73*, 3274.
(15) Sham, T. K.; Hastings, J. B.; Perlman, M. L. *J. Am.* Chem. *Soc.* **1980**, *102*. Sham, T. K.; Brunschwig, B. S. *Ibid.* **1981**, *103*, 1590.
(16) See ref 6 or: "X-ray Spectroscopy"; L. V. Azaroff, Ed.; McGraw-Hill, New York, 1974).
(17) Mott, N. F. *Proc. R. Soc. London, Ser.* A **1949**, *62*, 416. The relativistic effect of the core hole also modifies this considerably.
(18) McMaster, W. H.; Kerr Del Grande, N.; Mallett, J. H.; Hubbell, J. H. Compilation of X-ray Cross Sections, National Technical Information Service, Springfield, VA, 1969. The L-edge jumps are 3.431, 1.410, and 1.160 for L_{III}, L_{II}, and L_I, respectively.

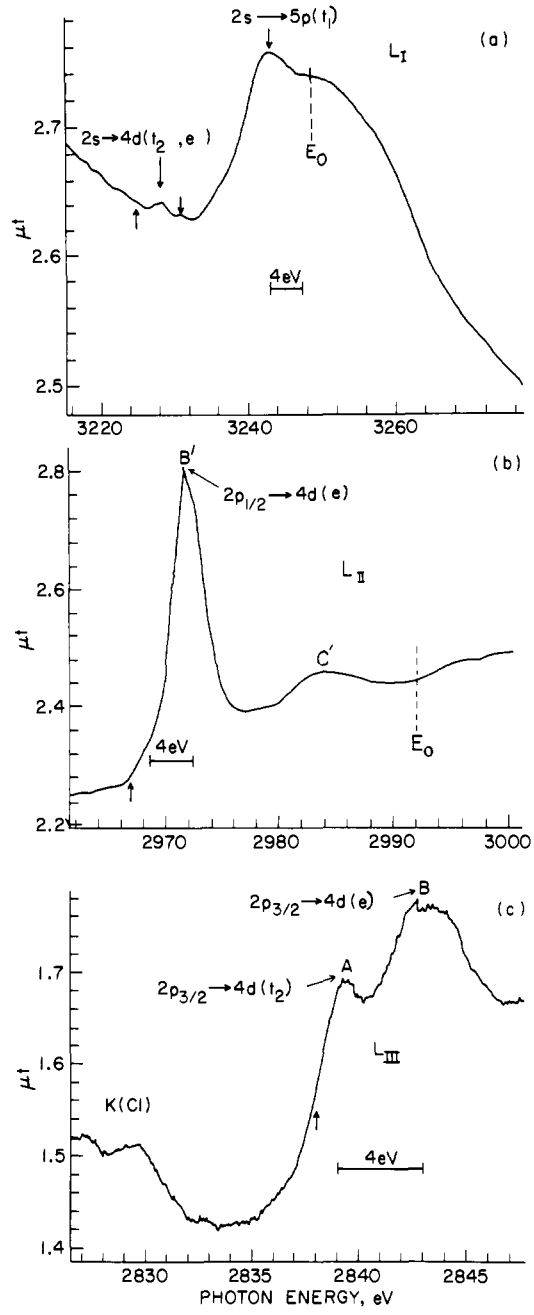

Figure 2. Near-edge region of $[Ru(NH_3)_6]Cl_3$: (a) Ru L_I, (b) Ru L_{II}, and (c) Ru L_{III}; B′ and A, B are transitions to the 4d final states (see text).

d_{xz}), and the 6σ orbitals of the ligand transform as A_1, E, and T_1 representations of the O point group. A molecular orbital diagram of the ground state is given in Figure 3 to illustrate the orbital symmetry. The dipole-allowed transitions are summarized in Table I, where the more common labels for the octahedral basis functions are also shown. It is apparent from Table I and Figure 3 that these transitions involve states of primarily metal character and that qualitative assignments can immediately be made. In the L_I spectrum the weak peak at ~3228 eV is tentatively assigned to the 2s → 4d quadrapole transition. The intense peak at 3242 eV is assigned to 2s → t_1 (Ru 5p character) transition. The separation between the first 2s → 4d and 2s → t_1(5p) from Figure 2 is ~14 eV, in qualitative accord with the atomic data[19] and atomic calculation.[20] What is perhaps the most interesting result

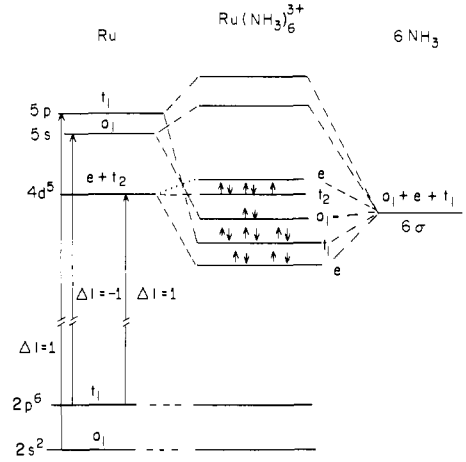

Figure 3. Simplified molecular orbital diagram of $Ru(NH_3)_6^{3+}$. Only local symmetry is considered; orbitals above $t_2(4d^5)$ are empty and those below are occupied. The corresponding atomic $\Delta l = \pm 1$ dipole allowed transitions are shown.

is that both the L_{II} and L_{III} spectra (Figure 2) show sharp white line structures (A, B, B′ in Figure 2) accompanied by a weak peak C and C′ for L_{II} and L_{III}, respectively, below E_0. While L_{II} has only one apparent sharp resonance, B′, L_{III} has two (A and B). All these absorption peaks are considerably narrower than the L_I edge 2s → t_1(5p) transition (half-width ~10 eV). Peaks A, B, and B′ are at first qualitatively assigned to 2p → (t_2, e) (Ru4d) transition, while C and C′ are assigned to 2p → a_1 (Ru5s) transition based on the dipole selection rules and the low-spin $4d^5$ configuration of $Ru(NH_3)_6^{3+}$ (a hole in the t_2 orbital). The difference in width between L_I and $L_{II,III}$ transitions is simply due to the intrinsic lifetime of the core holes.

L-Edge Bound-State to Bound-State Transition Intensity of Ru^{3+} in a Strong Crystal Field. The main concern here is to explain the observation that there is only one sharp resonance line (B′) at the L_{II} edge and a doublet (A,B) at the L_{III} edge. The first step is to align the E_0's for L_{II} and L_{III} with each other. This procedure allows us to conclude that B and B′ in Figure 2 are of the same nature (since B and B′ are in the same position defined by other peaks in the spectrum and have about the same width, ~4 eV). Peak A must arise either from contribution of the chlorine K-edge EXAFS or a transition involving spin consideration, which is allowed for the L_{III} edge and forbidden for the L_{II} edge. The former situation is very unlikely because (a) peak A (width ≃ 2.5 eV) is too sharp to be a chlorine K-edge EXAFS oscillation and (b) Cl^- is not symmetrically bonded in the lattice and the EXAFS oscillations should be weak due to static disorder. We must then consider the electron spin. This situation is somewhat analogous but not identical[24] with that of the Pt L edge. In Pt metal, white line is observed in the L_{III} ($p_{3/2}$) edge but not in the L_{II} edge. This anomaly has been attributed[6] to the $d_{5/2}$ character of the unoccupied d state ($\Delta m_j = 0, \pm 1$, selection rule).

To understand this anomaly, we have to calculate transition intensities between $2p_{j,mj}$ and the unoccupied valence levels of concern. To do this, final-state wave functions including spin need to be constructed by using the octahedral basis of the metal. The transition intensity of the absorption thus depends upon the dipole matrix element $\langle\psi_i|r|\psi_f\rangle$, where r is the dipole operator and ψ_i and ψ_f are the initial- and final-state wave functions (including spin), respectively. It is the detail of ψ_f that is important to the data analysis. Since $Ru(NH_3)_6^{3+}$ is d^5 low spin, it is appropriate to

(19) Moore, C. E. *Natl. Bur. Stand. (U.S.) Circ.* **1952**, *2*, A67.
(20) Ru^{3+} with configuration $4d^5$ is considered for transition calculations; $2p^{5.5}4d^{5.5}$ and $2p^{5.5}4d^{5.5}5s^{0.5}$ are used to represent 2p → 4d and 2p → 5s transitions, respectively.

(21) Endicott, J. F.; Taube, H. *J. Am. Chem. Soc.* **1962**, *84*, 4984. Creutz, C.; Taube, H. *Ibid.* **1973**, *95*, 1086.
(22) Jørgensen, C. K. *Acta Chem. Scand.* **1956**, *10*, 513.
(23) Griffiths, J. H. E.; Owen, J.; Ward, I. M. *Proc. R. Soc. London, Ser. A* **1953**, *219*, 526.
(24) In the Pt case the spin-orbit effect is large and $d_{5/2}$ and $d_{3/2}$ are reasonably well-defined even in a metal. In the Ru case, however, the spin-orbit effect is considerably smaller than the crystal field. Therefore $d_{5/2}$ and $d_{3/2}$ are not well-defined.

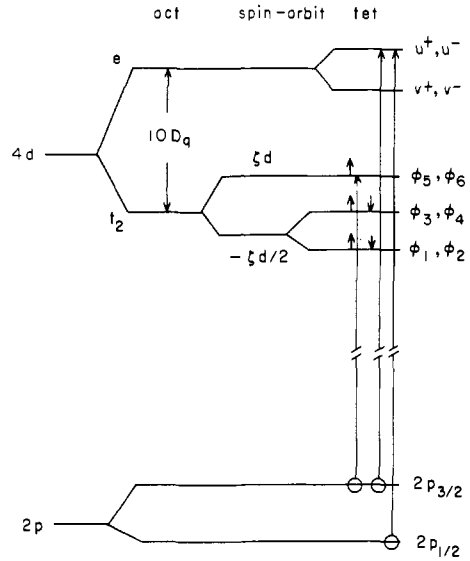

Figure 4. Energy diagram of $Ru(NH_3)_6^{3+}$, d^5 low-spin configuration in a strong crystal field; spin-orbit and tetragonal distortion are included. The energy levels are not to scale. The spin-orbit wave functions ϕ_1–ϕ_6 are in terms of the octahedral basis set and spin functions. The final-state spin-orbit core levels $p_{3/2}$ and $p_{1/2}$ are also shown together with transitions responsible for A′, A, and B.

treat this complex as a strong-field case. By introducing spin-orbit effects $H_1 = (\xi(r)L\cdot S)$ as the perturbation, the t_2 orbitals (ξ, η, ζ) are further split, and the corresponding new eigenfunctions ϕ_f (angular function in terms of spherical harmonics) are now linear combinations of ξ^+, η^+, ζ^+, ξ^-, η^-, and ζ^- where ξ^+ and ξ^- etc. represent spin-up $\xi(^1_0)$ and spin-down $\xi(^0_1)$ wave functions. A tetragonal (Jahn–Teller) distortion splits the spin-orbit levels further.[25] The ϕ_f functions and the energy diagram are shown in Figure 4. The total area of an absorption peak of a transition can be written[6] as

$$\text{area} = \int \mu(E)\mathrm{d}E = (2n_0\pi^2e^2\hbar/mc)\bar{f}_{if}n_h \qquad (1)$$

where n_0 is the number of Ru atoms per unit volume, n_h is the number of 4d holes, m is the mass of electron, c is the speed of light, and $\bar{f}_{if}$ is the average oscillator strength, the oscillator strength f_{if} is defined by eq 2, where $P_{n,l}$ and $P_{n,l\pm1}$ are related to the initial-

$$f_{if} = (2m\omega/\hbar)|\langle P_{n,l}|r|P_{n,l\pm1}\rangle|^2 = (2m\omega/\hbar)M_{if}^2 \qquad (2)$$

and final-state radial wave functions for a particular m_j value, with $(P_{n,l})/r$ etc. being the radial part of the single-particle wave function as given by the Herman–Skillman wave functions for Ru^{3+}. The average oscillator strength, $\bar{f}_{if}$, is the average of f_{if} amount different m_j's. The selection rule is determined by the angular part of the wave functions, i.e., the matrix elements $\langle\phi_{j,m_j}|\cos\theta|\phi_f\rangle$, where ϕ_{j,m_j} are initial-state wave functions expressed in terms of the spherical harmonics. For the 2p → 4d transition initiating from $p_{3/2,m_j}$ and $p_{1/2,m_j}$ we have

$$\phi_{p_{1/2,1/2}} = -(1/3)^{1/2}Y_{10}^{+} + (2/3)^{1/2}Y_{11}^{-} \qquad (3a)$$

$$\phi_{p_{1/2,-1/2}} = -(1/3)^{1/2}Y_{10}^{-} + (2/3)^{1/2}Y_{1-1}^{+} \qquad (3b)$$

$$\phi_{p_{3/2,3/2}} = Y_{11}^{+} \qquad (3c)$$

$$\phi_{p_{3/2,1/2}} = (2/3)^{1/2}Y_{10}^{+} + (1/3)^{1/2}Y_{11}^{-} \qquad (3d)$$

$$\phi_{p_{3/2,-1/2}} = (2/3)^{1/2}Y_{10}^{-} + (1/3)^{1/2}Y_{1-1}^{+} \qquad (3e)$$

$$\phi_{p_{3/2,-3/2}} = Y_{1-1}^{-} \qquad (3f)$$

(25) For details see: H. Watanbe "Operator Methods in Ligand Field Theory"; Prentice-Hall: Englewood Cliffs, NJ, 1966; p 102.

Table II. $|\langle\theta_{j,m_j}|\cos\theta|\phi_f\rangle|^2$ Values for Transitions from $p_{3/2}$, $p_{1/2}$ to ϕ_f[a]

O group symbol	$\lvert\langle\phi_{j,m_j}\rvert\cos\theta\rvert\phi_f\rangle\rvert^2$	m_j values $+^3/_2$	$+^1/_2$	$-^1/_2$	$-^3/_2$
t_2	$\lvert\langle\phi_{1/2,m_j}\rvert\cos\theta\rvert\phi_6\rangle\rvert^2$		0	0	
	$\lvert\langle\phi_{1/2,m_j}\rvert\cos\theta\rvert\phi_5\rangle\rvert^2$		0	0	
	$\lvert\langle\phi_{3/2,m_j}\rvert\cos\theta\rvert\phi_6\rangle\rvert^2$	0	0	0	$^1/_{10}\pi$
	$\lvert\langle\phi_{3/2,m_j}\rvert\cos\theta\rvert\phi_5\rangle\rvert^2$	$^1/_{10}\pi$	0	0	0
e	$\lvert\langle\phi_{1/2,m_j}\rvert\cos\theta\rvert\phi_{u^+}\rangle\rvert^2$		$^1/_{15}\pi$	0	
	$\lvert\langle\phi_{1/2,m_j}\rvert\cos\theta\rvert\phi_{u^-}\rangle\rvert^2$		0	$^1/_{15}\pi$	
	$\lvert\langle\phi_{3/2,m_j}\rvert\cos\theta\rvert\phi_{u^+}\rangle\rvert^2$	0	$^2/_{15}\pi$	0	0
	$\lvert\langle\phi_{3/2,m_j}\rvert\cos\theta\rvert\phi_{u^-}\rangle\rvert^2$	0	0	$^2/_{15}\pi$	0
a_1	$\lvert\langle\phi_{1/2,m_j}\rvert\cos\theta\rvert\phi_{a_1^+}\rangle\rvert^2$		$^1/_{12}\pi$	0	
	$\lvert\langle\phi_{1/2,m_j}\rvert\cos\theta\rvert\phi_{a_1^-}\rangle\rvert^2$		0	$^1/_{12}\pi$	
	$\lvert\langle\phi_{3/2,m_j}\rvert\cos\theta\rvert\phi_{a_1^+}\rangle\rvert^2$	0	$^1/_6\pi$	0	0
	$\lvert\langle\phi_{3/2,m_j}\rvert\cos\theta\rvert\phi_{a_1^-}\rangle\rvert^2$	0	0	$^1/_6\pi$	0

[a] Only u^+ and u^- values are given; all transitions to v^+ and v^- are zero; $a_1 = Y_{0,0}$.

Again Y_{lm}^+ and Y_{lm}^- represent spin-up $Y_{lm}(^1_0)$ and spin-down $Y_{lm}(^0_1)$ wave functions, respectively. ϕ_f's are the final-state wave functions. The explicit form of the ϕ_f's based on the t_2 basis set are

$$\phi_6 = -(1/3)^{1/2}(-\xi^- - i\eta^-) + (1/3)^{1/2}\zeta^+ \qquad (4a)$$

$$\phi_5 = (1/3)^{1/2}(\xi^+ - i\eta^+) - (1/3)^{1/2}\zeta^- \qquad (4b)$$

$$\phi_4 = (-\xi^+ - i\eta^+)/2^{1/2} \qquad (4c)$$

$$\phi_3 = (\xi^- - i\eta^-)/2^{1/2} \qquad (4d)$$

$$\phi_2 = (1/6)^{1/2}(-\xi^- - i\eta^-) + (2/3)^{1/2}\zeta^+ \qquad (4e)$$

$$\phi_1 = (1/6)^{1/2}(\xi^+ - i\eta^+) + (2/3)^{1/2}\zeta^- \qquad (4f)$$

where ξ, η, ζ, etc. are in terms of spherical harmonics (Table I). The e-basis wave functions are not split by spin-orbit effects. The matter now remaining to be dealt with is the following integral (eq 5) in terms of which the matrix elements $\langle\phi_{j,m_j}|\cos\theta|\phi_f\rangle$ can be calculated. Results of the evaluation of eq 5[26] relevant to the assignment of the near-edge structure are given in Table II.

$$\langle Y_{lml}|\cos\theta|Y_{l'm'l'}\rangle = (-1)^{ml}\left[\frac{3(l+1)(2l'+1)}{4\pi}\right]^{1/2}\begin{pmatrix} l & 1 & l \\ -ml & 0 & ml\end{pmatrix}\begin{pmatrix} l & 1 & l' \\ 0 & 0 & 0\end{pmatrix} \qquad (5)$$

What immediately emerges from Table II is that the dipole transition to the empty t_2 state, ϕ_6 in Figure 4, can only arise from the $p_{3/2}$ state while the e states (u^+ and u^- in Figure 5) can be reached by both the $p_{3/2}$ and $p_{1/2}$ states. We therefore expect the 2p → 4d transitions to be split at the L_{III} edge, primarily by the octahedral field ($10Dq$), while only one intense 2p → 4d transition is expected at the L_{II} edge. The experimental results (Figure 2) show that this is indeed the case. Quantitatively, the observed splitting ΔE at the L_{III} edge should account for the strength of the crystal field ($10Dq$) and the spin orbit interaction ($\zeta_d = \langle Y_{lm}|\xi(r)|Y_{lm}\rangle$). Tetragonal interaction is assumed to be negligible as indicated by X-ray and EXAFS data. If the final-state relaxation is considered to be the same for the split $4d^5$ levels we can write

$$\Delta E(\text{eV}) = 10Dq - \zeta_d \qquad (6)$$

Using tabulated[27] ζ_d of 0.13 eV and the observed ΔE of 3.8 eV (33 600 cm^{-1}), we calculated a $10Dq$ value of 3.93 eV, which is in reasonable agreement with the usual $10Dq$ value for Ru^{III} and

(26) The 3j values can be found in: "The 3 – j and 6 – j Symbols"; M. Rotenberg, R. Bivins, N. Metropolis, J. Wooten, Jr., Eds.; The Technology Press: M.I.T., Cambridge, MA, 1959.

(27) Griffith, J. S. "The Theory of Transition-Metal Ions"; Cambridge University Press: New York, 1961.

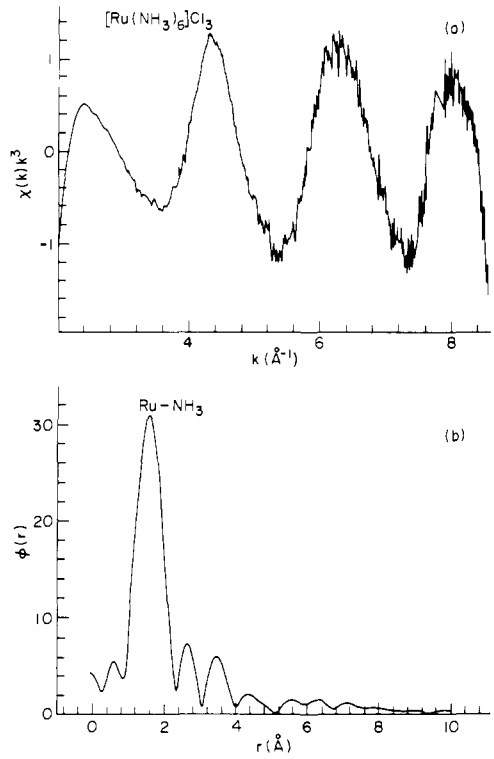

Figure 5. (a) χk^3 (raw data) and; (b) Fourier transform of $Ru(NH_3)_6Cl_3$ L_I-edge EXAFS.

Rh^{II} compounds.[28] The relative ratio of peak intensity

$$I(B)/I(A) = \bar{f}_{if}(B)n_h(p_{3/2} \rightarrow \phi u)/\bar{f}_{if}(A)n_h(p_{3/2} \rightarrow \phi_6)$$

is calculated to be 8/3 = 2.7 (assuming identical radial matrix elements), in good agreement with the observed 3.0 ± 1 (depending on background subtraction). The narrower width of A compared with B is most likely due to the fact that ϕ_6 is a localized nonbonding orbital while u^+ and u^- are more delocalized, involving some ligand character (Figure 3).

We now consider the transitions C and C′. Take the L_2 edge, for example. When Herman–Skillman wave functions are used with a local statistical density potential, the energy difference between the 2p → 4d and the 2p → 5s transition in the Ru^{3+} ion is calculated to be 6.8 eV suggesting that the 4d states are tighter bounded. This result is consistent with the assignment of peaks C and C′ being most probably the 2p → 5s transition. The separation between B′ and C′ is 12 eV, supporting the assignment made for the L_I edge. It is worth mentioning that d → d transitions in this type of complex are often obscured in the optical spectrum by intense charge-transfer absorption.[22,23] It would appear then that L-edge X-ray absorption may be useful for crystal-field studies. Peaks D and D′ lie in the most troublesome region; they are either shape-resonance states[14] or the beginning of the EXAFS.[1]

L_I-Edge EXAFS. We now turn to the L_I EXAFS. Once background is substracted and the data are weighted with k^3 the EXAFS[1] (eq 7) can be clearly seen (Figure 5a), μ is the absorption

$$\chi(k) = (\mu - \mu_0)/\mu_0 = \sum(-N_i|f(\pi,k)|/kr_i^2)e^{-2\sigma_i^2k^2}e^{-2r_i/\lambda} \sin [2kr_i + \phi(k)] \quad (7)$$

coefficient, μ_0 the smoothed absorption of an isolated atom, k the electron wave number ($k = [2m(E - E_0)]^{1/2}h$), N_i the coordination number, σ_i^2 the root-mean-square deviation of r_i, and λ the electron mean free path. It is apparent from eq 7 that with the knowledge of the phase $\phi(k)$ and the amplitude $f(\pi,k)$ of the absorbing and the scattering atoms, r_i and σ_i^2 can be extracted from the experimentally obtained $\chi(k)$[1]. The Fourier transform (Figure 5b) of the truncated data clearly shows a peak. By use of the theoretical phase shifts given by Teo and Lee,[8] a value of Ru–N = 2.10 ± 0.02 Å is obtained as an average of various fits due to different k^2 and k^3 weighting and truncation. The Ru–NH_3 bond length given by X-ray crystal structure[29] of $[Ru(NH_3)_6](BF_4)_3$ is 2.104 ± 0.004 Å. It is clear that the r(Ru–N) from EXAFS is in reasonable agreement with the X-ray diffraction result.

Conclusion

I have presented Ru L-edge spectra of $[Ru(NH_3)_6]Cl_3$ with semiquantitative interpretation. It appears that Ru L-edge absorption spectra are rich in structure. More important, these absorption structures are final-state selective and sensitive to spin orbit effects and thus are very informative about the symmetry and the electronic properties of the unoccupied molecular orbitals.[30] These empty states play very important roles in chemical reactions. Since the initial state is exclusively atomic-like, ligand to metal charge transfer would not interfere at the metal edge and the technique should be complementary to UV–visible spectroscopy.

Acknowledgment. I thank Dr. B. S. Brunschwig for his assistance in the measurements and Dr. J. Davenport for making his Herman–Skillman program available. I am particularly grateful to Dr. R. E. Watson for his suggestions in the evaluation of the transition matrix elements and discussion. The research was carried out at Brookhaven National Laboratory under contract with the U. S. Department of Energy and supported by its Office of Basic Energy Science. Work done at SSRL, which is supported by the NSF through the Division of Materials Research and the NIH through the Biotechnology Resource Program in the Division of Research Resources (in cooperation with the Department of Energy), is acknowledged.

Note Added at Proof. Recently Horsley[31] indicated that some of the unoccupied d states in IrO_2 might not have been measured by the resonance transition. Considering the electronic configuration, the local geometry, and the analysis presented here, this absence of intensity is not unexpected.

Registry No. $[Ru(NH_3)_6]Cl_3$, 14282-91-8.

(28) The $10Dq$ for $Ru(NH_3)_6^{3+}$ is not known, but the $10Dq$ for $Rh(NH_3)_6^{3+}$ is 34000 cm^{-1} Schmidtke, H. H. *J. Mol. Spectrosc.* **1963**, *11*, 483.

(29) Stynes, H. C.; Ibers, J. A. *Inorg. Chem.* **1971**, *10*, 2304.

(30) It must be noted that if we assume the final-state relaxation for both transitions to be the same the splitting in $Ru(NH_3)_6^{3+}$ (L_3 edge) should approximate $10Dq - \zeta d$. In the context of equivalent core approximation one may think that the first transition results in a final state equivalent to $Rh(NH_3)_6^{3+}(t_2^6)$. The second transition, however, corresponds to an excited state of $Rh(NH_3)_6^{3+}(t_2^5,e^1)$. Therefore, the L_3-edge splitting is also equivalent to $10Dq - \zeta d$ for $Rh(NH_3)_6^{3+}$.

(31) Horsley, J. A. *J. Chem. Phys.* **1982**, *76*, 1451.